Wegrzyn, M.; Sahuquillo, O.; Benedito, A.; Giménez Torres, E. (2015). Morphology, Mechanical Performance and Nanoindentation Behavior of Injection Molded PC/ABS-MWCNT Nanocomposites. Journal of Applied Polymer Science. 132(22):1-8. https://doi.org/10.1002/app.42014

WILEY Journal of Applied Polymer Science

Morphology, Mechanical Performance and Nanoindentation Behavior of Injection Molded PC/ABS-MWCNT Nanocomposites.

Journal:	*Journal of Applied Polymer Science*
Manuscript ID:	APP-2014-02-0731.R2
Wiley - Manuscript type:	Research Article
Keywords:	blends, morphology, nanotubes, graphene and fullerenes, mechanical properties, molding

GRAPHICAL ABSTRACT

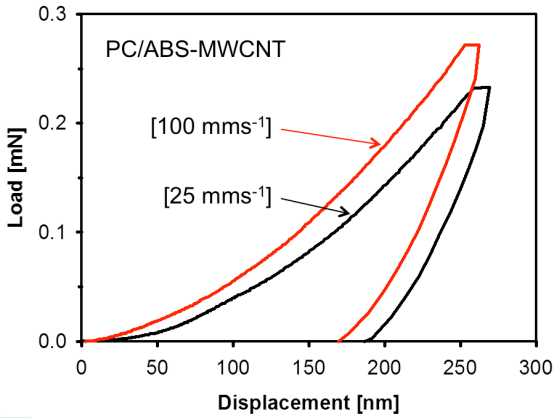

Morphology, Mechanical Performance and Nanoindentation Behavior of Injection Molded PC/ABS-MWCNT Nanocomposites

Marcin Wegrzyn [a], Oscar Sahuquillo [b], Adolfo Benedito [a], Enrique Gimenez [b]

[a] Instituto Tecnológico del Plástico (AIMPLAS), Calle Gustave Eiffel 4, 46980 Paterna, Spain

[b] Instituto de Tecnología de Materiales. Universidad Politécnica de Valencia, Camino de Vera, 46022 Valencia, Spain

Correspondence to: Marcin Wegrzyn (E-mail: *marcinwegrzyn@hotmail.com*)

ABSTRACT

In this work, nanocomposites of polycarbonate/acrylonitrile-butadiene-styrene (PC/ABS) with various loads of multi-wall carbon nanotubes (MWCNT) are investigated. Material is previously formed by masterbatch dilution approach and further processed by injection molding at two injection velocities: 25 mms^{-1} and 100 mms^{-1}. Characterization of nanocomposites morphology by transmitted light- and transmission electron microscopies shows the dependence of MWCNT dispersion on processing parameters and nanofiller load. Nanocomposite homogeneity on various distances from the injection gate is studied by Raman spectroscopy. Mechanical properties, improved with the addition of MWCNT, are studied by tensile testing and nanoindentation. The results agreement between uniaxial tensile testing and nanoindentation show a slight decrease of nanocomposites' mechanical performance at 3.0 wt. % MWCNT in samples injected at 25 mms^{-1}. This is related to increased agglomeration behavior at these conditions.

KEYWORDS

Blends; Morphology; Nanotubes, Graphene and Fullerenes; Mechanical Properties; Molding.

INTRODUCTION

Unique structure and excellent properties of carbon nanotubes (CNT) resulted with advanced technological applications of this material, mainly as a reinforcement of polymer composite

materials. This application has attracted interest of researchers and scientists in recent years due to the superior electrical and mechanical properties of carbon nanotubes. [1,2] Due to their high surface energy, high aspect ratio and strong van der Waals force, CNT show a tendency to form agglomerates. Therefore, effective use of carbon nanotubes in composite applications depends strongly on the ability to disperse the nanofiller homogeneously in the matrix, without destroying the integrity of the individual nanotubes. Furthermore, immiscible polymeric blends, recently more often employed as a matrix for nanocomposites, [3,4] offer noticeable reduction of nanofiller loading for performance comparable with single-phase matrices. Multiphase matrices bring some additional questions in topics related to morphology, *e.g.* selective location of nanofiller in one phase [3,4] or the necessity of the presence of co-continuous morphology for electrical reinforcement. [5] Proper conditions during nanocomposite formation [1] and processing [6] have to be selected in order to reduce the agglomeration problem by an effective agglomerate penetration by polymer melt. The appearance of primary- and secondary agglomerates [7] in industrially produced nanocomposites is relatively well controlled in a masterbatch dilution process. [5,8]

Among several types of melt mixing processes in nanocomposite preparation, extrusion process has captured considerable interest. This is due to its industrial importance and a relatively good understanding of carbon nanotubes dispersion in polymer matrix. [8] In case of other processes, *e.g.* injection molding commonly used in industry, this precise knowledge of the dispersion behavior is incomplete. Moreover, a lower homogeneity of carbon nanotubes dispersion is reported in the majority of scientific literature after injection molding than after compounding. Rather high dependence of the final properties on the processing parameters is required. [9-11]

Additional variables present in the material manufacturing process, such as the geometry of the specimen, determine the concentration of the nanofiller in various parts of the specimen [12,13] regarding the distance of the specimen walls and injection gate location. Shear-induced melt flow influencing carbon nanotubes entanglement can be controlled by melt temperature [14] and injection velocity. [10] Moreover, the orientation of carbon nanotubes and the presence of skin-effect as a consequence of the high-shear processing conditions used in injection molding is reported by other groups. [10,11] Some dynamic injection molding techniques are used in order to improve the control of the nanofiller orientation. [15] Therefore, the relation between MWCNT orientation and location in the specimen can be controlled by the processing parameters.

The industrial control of the nanofiller dispersion and its influence on the mechanical properties is commonly carried out in industry by tensile testing. Nevertheless, the tensile testing has some limitations in determining the microscopic interactions in nanocomposite materials. In this regard, the nanoindentation test provides a new opportunity for studying the mechanical properties in sub-micrometer scale. [16] Along Young's modulus, that can be also determined from tensile testing, hardness and plasticity index are commonly calculated from nanoindentation tests due to the development of modeling methods. [16] Among the various techniques available for polymers (*e.g.* use of different intender tip type), a Continuous Stiffness Measurement (CSM) mode has been revealed as a suitable technique for measuring elastic modulus and hardness at small working depths. [17-21] In the conventional Nanoindentation mode stiffness is usually determined by analyses of the unloading curve, following the Oliver and Pharr method. [17-19,22-24] The CSM mode enables the instrument to

determine contact stiffness throughout the experiment during the loading segment of the curve. [17,20,21,25]

In this work, we present evaluation of mechanical properties of injection molded PC/ABS-MWCNT nanocomposite introduced elsewhere. [26] We now report the close study of the quality of carbon nanotubes dispersion in polymer matrix characterized by transmitted light microscopy (OM), transmission electron microscopy (TEM) and Raman spectroscopy. Quality of morphology, regarding carbon nanotube agglomeration and location of carbon nanotubes in injection molded sample, was related with the study of mechanical performance. Uniaxial tensile testing and nanoindentation representing respectively macro- and microscopic behavior, showed the importance of homogeneous distribution of nanofiller in nanocomposite material.

EXPERIMENTAL

Materials

Polycarbonate/acrylonitrile-butadiene-styrene (PC/ABS) commercial blend Bayblend® T85 was supplied by Bayer MaterialScience. Polycarbonate content is 85 wt. %, MVR is 12 cm^3/10 min and Vicat softening temperature is 129 ºC (data provided by supplier). Nanofiller: multi-walled carbon nanotubes (MWCNT) NC7000, was supplied by Nanocyl. Average diameter of individual tube is 9.5 nm and average length 1.5 µm (data provided by supplier).

Preparation of nanocomposites

Nanocomposites were formed with pre-dispersed 5 wt.% MWCNT masterbatch dilution on a twin-screw co-rotating laboratory extruder Prism Eurolab 16 (Thermo Fisher Scientific) with length-to-diameter ratio (L/D) 25. Nanocomspoite samples were obtained according to previously reported conditions. [27] Throughput during production and dilution of masterbatch was 1 kgh^{-1} with barrels temperature 280ºC and screw speed 400 rpm.

Final nanocomposites of MWCNT concentrations between 0.5 wt.% and 3.0 wt.% were injection molded on BOY Spritzgiessautomaten 12A at 280ºC with mold temperature of 70ºC and two injection velocities: 25 mms^{-1} and 100 mms^{-1}. Samples with two different geometries were used in this study. Dog bone samples prepared according to the standard EN ISO-527-3 and rectangular specimens with dimensions 60x10x3 mm^3 (following modified standard ISO 127).

Characterization

Morphology of the nanocomposites was studied by transmitted light microscopy (OM) on Leica DMRX microscope, Slices 20-50 µm thick were cut from the cross section of the rectangular specimen. Transmission electron microscope (TEM) used in this study was JEOL JEM-1010 with electron gun at 100kV and a MegaView III digital camera. Samples were prepared on a copper grid (300 mesh) and coated with carbon film. Raman spectroscopy measurements were done on Horiba XploRA with 532nm laser LCM-S-11 and CCD detector.

Tensile testing was performed according to ASTM D-638 on an Instron Universal Machine 3343 with 5kN load cell and a speed of 5mm min^{-1}. Experiments were done at constant conditions: 50±5% HR and 24±2ºC.

Nanoindentation tests were carried out using a G-200 nanoindenter from Agilent Technologies with a Berkovich diamond tip, previously calibrated on standard silica. Tip was pushed into the material until 250 nm depth was reached, the force was maintained for 5 s and released. Measurements were carried out in nine different points for each sample separated by 120 μm. Stiffness used for evaluating mechanical properties was calculated by a Continuous Stiffness Measurement mode (CSM) set at 45 Hz oscillation frequency and 2 nm harmonic oscillation amplitude at a strain rate of $5x10^{-2}$ s^{-1}. Plasticity index Ψ was calculated with Equation 1 [28], where A_1 is the area under the curve recorded during loading (intender pressing into the material) and A_2 is the area under the curve recorded during unloading (intender removing step).

$$\Psi = \frac{A_1 - A_2}{A_1} \quad (1)$$

RESULTS AND DISCUSSION

Dispersion and location of carbon nanotubes

The morphology of injection-molded nanocomposites was investigated using transmitted light microscopy. Figure 1 shows the OM images of the PC/ABS with 0.5 wt. % MWCNT obtained

previously by masterbatch dilution. The study of MWCNT dispersion in PC/ABS nanocomposites prepared by melt mixing was previously reported by the authors thus the morphology of nanocomposites after a twin-screw extrusion process is not described here. [26] The images for OM study were collected from the cross-section of the sample area near the injection gate. A relatively homogeneous dispersion of carbon nanotubes with a minor degree of agglomeration was achieved for both studied injection velocities. Nevertheless, lower agglomeration in the central part of the cross-section was observed for lower injection velocity. Higher concentration of carbon nanotubes, observed as a darker area (Figure 1a), was also present in the central part of the cross-section of the sample injected at 25 mms^{-1}. Higher injection velocity of 100 mms^{-1} (Figure 1b) resulted in an increase of agglomerate number distributed homogeneously in the whole sample. This flow-induced agglomeration coalescence should occur in each studied injection velocity, but at 25 mms^{-1} it is effectively balanced by a flow-induced agglomerated destruction. This competition between flow-induced effects, if understood, allow propezr control of the specimen morphology. Moreover, a layered structure is present at elevated injection velocity with darker areas most probably related to MWCNT-rich zones. Such separation occurs with significantly lower intensity also at 0.5 wt. % MWCNT, which can be understood as a gradient of carbon nanotubes concentration increasing towards the core of the specimen. Intensification of this effect present at 100 mms^{-1} is related to high shear stress and changes in the characteristics of the flow of discrete polymer layers.

The increase of carbon nanotubes load to 1.0 wt. % (Figure 2) resulted in an increase of agglomerate number and the reduction of the sensitivity to injection velocity. A rather homogeneous distribution of agglomerates in the whole cross-section occurs for both: 25

mms^{-1} and 100 mms^{-1}. Such behavior is correlated with the increase of melt viscosity occurring at higher nanofiller loads, causing only a slight increase of agglomeration with shear. Moreover, MWCNT gradient observed at various distance from the core of the sample seems to be reduced when compared to lower nanofiller load.

Figure 3 shows the TEM micrograph of a 1.5 wt. % MWCNT nanocomposite injection molded at 100 mms^{-1}. Preferential location of carbon nanotubes in polycarbonate observed in Figure 3 was reported earlier. [3] Injection molding with higher shear applied to the material seems to have no effect on the location of carbon nanotubes due to more transporting than mixing character of the screw in injection molding machine. Furthermore, Figure 3 suggests strong carbon nanotubes chopping during applied processing path showing also low orientation of the shortened tubes. This is because the cross-section of the sample was subtracted in the direction perpendicular to the melt flow, so eventual orientation of the nanotubes cannot be observed. Besides, only minor part of the actual size of individual MWCNTs can be observed in Figure 3 indicating short size of the structure due to the processing. Therefore, no conclusions regarding shortening MWCNT can be made.

A further study of MWCNT distribution in the injection-molded specimen was done by Raman spectroscopy on rectangular bars prepared as shown in Figure 4a. The injection gate area is marked with a letter A while the opposite end of the specimen is an E. Spectrum was recorded from a cross-section of each of the five elements. The central area of the specimen and the side areas were investigated (Figure 4b) to see the differences along the width and length of the sample. Figure 5 shows the results of this investigation in the form of D-to-G peak intensities

ratio for various positions in the specimen. These peaks appear in vibrational spectra at 1347 cm^{-1} and 1599 cm^{-1}, respectively. [29] A slight blue shift of these bands compared to the pristine multi-wall carbon nanotubes (1340 cm^{-1} and 1575 cm^{-1}, respectively) is a result of the disentanglement and was reported in earlier studies. [30] The reason of selection of the D/G intensity parameter instead of direct analysis of each peak is related to overlapping of the G-band and the band at 1500 cm^{-1}. Therefore, D/G intensities ratio seems to be a representative parameter showing the balance between MWCNT shortening (D-band as a MWCNT defect indicator) and orientation, especially assuming the similar agglomeration behavior above 1.0 wt. % MWCNT for both velocities, observed in Figure 2. Reduced injection velocity 25 mms^{-1} gives clearly lower value of D/G parameter than the 100 mms^{-1}. Moreover, the homogeneity of the sample along and across the flow direction seems to be higher at elevated injection velocities. This can be related to the higher orientation of carbon nanotubes and more uniform length distribution in the sample cavity at 100 mms^{-1}. Values of D/G intensities in the direction perpendicular to the melt flow form the opposite pattern for low- and high injection velocities. Higher mobility of shortened carbon nanotubes explained by greater flow ability of such structures compared to the higher aspect ratio structures can be responsible for such effect. Besides, the temperature of nanocomposite melt and the temperature of internal mold surfaces differ significantly. At various injection speed the contact between these two surfaces causing temperature exchange affects the orientation of the nanomaterial. High injection velocity provides higher shear between the cooled down material that is in the direct contact with the mold wall and moving material, which allows higher orientation of the nanotubes. The frozen layer at 25 mms^{-1} forming skin effect should be thicker and contain less oriented

nanotubes due to lower speed of fountain flow propagation. Slow fountain flow propagation is also affecting the MWCNT orientation state along the direction of the flow, which appears as increasing of the D/G ratio for 25 mm s^{-1} in Figure 5. Regarding this, 25 mms^{-1} results with higher orientation in the sample core area, while 100 mms^{-1} shows higher D/G intensities values for side regions. Furthermore, longer time of mold filling in the former case allows more relaxation than it is possible for elevated injection velocity.

Tensile testing results

Mechanical properties of injection molded PC/ABS-MWCNT nanocomposites with various carbon nanotube loads were studied by tensile testing on dog-bone samples. Figure 6 shows Young's modulus values obtained during the tensile testing as a function of MWCNT loading. Stiffness increases 15-20 % with carbon nanotubes load until 3.0 wt. % for both injection velocities with slightly higher values at 100 mms^{-1}. The improvement of stiffness seems to reach the plateau at 1.0 wt. % MWCNT for both applied processing conditions. Above this point the improvement of Young's modulus is clearly lower. The effect of carbon nanotubes concentration is most probably related to the increase of nanocomposite melt viscosity above 1.0 wt. % MWCNT, which reduces motion freedom of the individual carbon nanotubes. Higher values of Young's modulus obtained for nanocomposites processed at higher injection speed (100 mm s^{-1}) can be related with a higher carbon nanotubes orientation degree, which is corroborated with Raman spectroscopy results. Furthermore, anisotropic tensile modulus is

known to be influenced by processing parameters when macro- or nano-scale fillers are used. [31,32]

Yield stress results shown in Figure 7 presents similar behavior to Young's modulus with higher values at elevated MWCNT load and injection velocity. The influence of the injection speed is also observed for pristine matrix and amplified when the nanofiller is introduced. Furthermore, the same carbon nanotube concentration of 1.0 wt. % appears to be the point where the plateau begins. Elongation at break (Figure 8) slightly decreases with MWCNT load and higher values are obtained at lower injection velocity for the whole carbon nanotubes range. Plateau for this parameter was observed between 0.5 wt. % and 2.0 wt. % MWCNT, which can be explained by the range of nanofiller where a similar agglomeration behavior for the same injection velocity is obtained. Agglomerates formation within this range is most probably controlled by the balance between MWCNT load and the increase of melt viscosity caused by higher number of nanotube-polymer chains interactions. Nanofiller concentrations above 2.0 wt. % promote the formation of agglomerates that cannot be broken. Decrease of ductility at higher injection velocity was reported earlier on pristine polymer [33] and is related to the orientation of polymer chains and fillers. At elevated injection velocities the chains and the individual carbon nanotubes are tightly packed and have relatively high orientation degree providing mechanical reinforcement. Such anisotropy reduces absorbed energy and increases brittleness of the nanocomposite.

Nanoindentation results

Figure 9 shows typical loading-hold-unloading curves of neat PC/ABS and its nanocomposites as a function of MWCNT content. On loading, the force is incremented at constant velocity. The curves shift upwards with increasing MWCNT concentration, indicating that the nanocomposite resistance to indentation gradually increases with nanomaterial load. This increase is higher for the PC/ABS nanocomposites injection molded at high injection speed 100 mms^{-1} (Figure 9b) than at 25 mms^{-1} (Figure 9a). Nanocomposite with 3.0 wt. % MWCNT processed at 25 mms^{-1} shows performance similar to the virgin PC/ABC. This effect is related with the increased agglomeration of carbon nanotubes in these conditions. Even though the tensile testing shows no influence of the decrease of morphology quality at elevated nanofiller loads, the nanoindentation reveals the decrease of mechanical properties. This observation seems to be opposite to the results shown in Figure 1, where the agglomeration increases at 100 mms^{-1} rather than at 25 mms^{-1}. However, the fair part of secondary agglomerates formed during the nanocomposite processing at low injection velocity is in the nano-size rather than in a micron-size. Therefore, high MWCNT load affects the load-unload curves in nanoindentation – method sensitive enough to detect this effect. A non-homogeneous distribution of the agglomerate size may be responsible for this effect as well.

Depths of the nanointender penetration represent the contributions from both, elastic and plastic displacements. The loading curves are followed by a 5 second period of holding time, during which the loads are constant. Next, the elastic displacements are recovered when the load force is reduced. A displacement associated with creep mechanisms in the maximum holds segments for both neat PC/ABS and the nanocomposites are observed.

Figure 10 and Figure 11 show changes of hardness and elastic modulus as a function of MWCNT concentration for both injection speeds (25 and 100 mms^{-1}). An enhancement of hardness and stiffness with the increase of carbon nanotubes content is shown. This is related with the intrinsic strength and high aspect ratio of individual carbon nanotubes. The overall enhancement is higher for samples processed at higher injection speed (100 mms^{-1}). [23] These results are consistent or comparable with the trend observed previously for the modulus values obtained by uniaxial tensile tests. When compared with the neat PC/ABS, the nanocomposites containing 3.0 wt. % MWCNT show in both methods c.a. 15 % increase of Young's modulus at low injection speed (25 mms^{-1}). An increase of hardness for optimal load of 1.5 wt. % MWCNT shows approximately 29 % and 10 % obtained for samples processed at 25 mms^{-1} and 100 mms^{-1}, respectively. Such behaviour was reported earlier for other polymers. [23,24] The increase of hardness (Figure 11) indicates higher material resistance against the deformation caused by a normal load.

The nanoindentation properties (Young's modulus and hardness) for sample with 3.0 wt. % MWCNT content processed at 25 mms^{-1} decrease slightly in comparison with the sample injected at 100 mms^{-1}. This decrease was not observed in the modulus measurements carried out by tensile tests. The differences may be caused by the non-homogeneous distribution of the agglomerates (*e.g.* wide agglomerates size distribution) (Figure 2a). Therefore, the nanoindentation tests are inadequate for inhomogeneous materials when the characteristic size of inhomogeneity (*e.g.* agglomerate) is of the same order of magnitude as the lateral dimensions of the indentation. [34] It is not possible to obtain the effective elastic properties for such materials. A disagreement between uniaxial tensile tests and nanoindentation data was

previously reported for epoxy matrix composites with graphite platelets [34] and carbon nanotube composites. [35] It was attributed to dissimilar material response in tension and compression that stems from the complex loading profile applied in indentation.

The plasticity index is understood as a ratio of the area enclosed between the loading-unloading curves to the area under the loading curve. [36] For a perfectly plastic material plasticity index is 1, while for viscoelastic material it is ranging between 0 and 1. Plasticity index presented in Figure 12 decreases with the addition of MWCNT, indicating the improvement in elastic recovery of nanocomposites after removing the external load. The samples processed at higher injection speeds (100mm^{-1}) show lower values of plasticity index due to a higher stiffness and orientation of carbon nanotubes. A similar behaviour was reported for epoxy-based vinyl-ester polymer matrix with graphene nanoplatelets. [23] An unusual increase of plasticity index for 3.0 wt. % MWCNT at 25 mms^{-1} is observed. This confirms the agglomeration of the carbon nanotubes at elevated loads [24,25] caused by the low injection velocity.

CONCLUSIONS

In this study, morphology and mechanical behavior of PC/ABS-MWCNT nanocomposites with different concentrations of carbon nanotubes processed at two injection velocities (25 mms^{-1} and 100 mms^{-1}) were investigated. Relatively homogeneous dispersions of carbon nanotubes with a minor degree of agglomeration were achieved for both studied injection speeds and the lowest agglomeration was observed for the low MWCNT content (0.5 wt. %) injection molded at 100 mms^{-1}. D/G intensities ratio in Raman spectra demonstrated that the dispersion of

carbon nanotubes along and across the flow direction was more homogeneous at elevated injection velocity. Besides, the Raman spectroscopy results appear as a good tool to study orientation and localization of carbon nanotubes in injection molded specimen.

The trend in tensile test results shows that MWCNT improve the mechanical properties of PC/ABS especially at low weight fractions. Stiffness and yield stress increases with carbon nanotubes load until 3.0 wt. % for both injection velocities with slightly higher values observed at 100 mms^{-1}. On the other hand, increase of MWCNT content causes a reduction of elongation properties due to the agglomeration of nanotubes.

The Young's modulus values obtained by nanoindentation are comparable with those obtained from tensile tests. A higher increase of stiffness and hardness was observed for nanocomposites processed at high injection velocity (100 mms^{-1}) when compared with the samples injected at 25 mms^{-1}. The indentation data is suitable for obtaining an effective elastic moduli and hardness values when the surface area of agglomerates is much smaller than the contact area of the indenter. In the particular case of nanocomposites with 3.0 wt. % MWCNT injected at low velocity (25 mms^{-1}), where a non-homogeneous dispersion of carbon nanotubes is obtained, the nanoindentation properties (Young's modulus and hardness) decreased slightly when compared with the sample injected at 100 mms^{-1}. This effect was not observed in macro-scale tensile tests.

ACKNOWLEDGEMENTS

This work is funded by the European Community's Seventh Framework Program (FP7-PEOPLE-ITN-2008) within the CONTACT project Marie Curie Fellowship under grant number 238363.

REFERENCES

1. Alig, I.; Lellinger, D.; Engel, E.; Skipa, T.; Pötschke, P. *Polymer* **2008**, 49, 1902-1909.
2. Sathyanarayana, S.; Wegrzyn, M.; Olowojoba, G.; Benedito, A.; Gimenez, E.; Hübner, C.; Henning, F. *Express Polymer Lett.* **2013**, 7, 621-635.
3. Xiong, Z.Y.; Wang, L.; Sun, Y.; Guo, Z.X.; Jian, Y. *Polymer* **2013**, 54, 447-455.
4. Sun, Y.; Gou, Z.X.; Yu, J. *Macromol. Mater. Eng*. **2012**, 295, 263-268.
5. Göldel, A.; Kasaliwal, G.; Pötschke, P.; Heinrich, G. *Polymer* **2012**, 53, 411-421.
6. Tiusanen, J.; Vlasveld, D.; Vourinen, J. *Comp. Sci. Technol.* **2012**, 72, 1741-1752.
7. Ma, P.C.; Siddiqui, N.A.; Marom, G.; Kim, J.K. *Composites A* **2012**, 41, 1345-1367.
8. Sathyanarayana, S.; Olowojoba, G.; Weiss, P.; Calgar, B.; Pataki, B.; Mikonsaari, I.; Huebner, C.; Hening, F. *Macromol. Mater. Eng*. **2013**, 298, 89-105.
9. Pegel, S.; Pötschke, P.; Petzold, G.; Alig, I.; Dudkin, S.M.; Lellinger, D. *Polymer* **2008**, 49, 974-984.
10. Villmow, T.; Pegel, S.; Pötschke, P.; Wagenknecht, U. *Compos. Sci. Technol*. **2008**, 68, 777-789.
11. Richter, S.; Saphiannikova, M.; Jehnichen, D.; Bierdel, M.; Heinrich, G. *Express Polym. Lett*. **2009**, 3, 753-768.
12. Park, D.H.; Yoon, K.H.; Park, Y.B.; Lee, J.D.; Lee, Y.J.; Kim, S.M. *J. Appl. Polym. Sci.* **2009**, 113, 450-455.
13. Chandra, A.; Kramschuster, A.J.; Hu, X.; Turng, S. *Proc. Annual Technical conference of the Society of Plastics Engineers* **2007**, 3, 2184-2188.

14. Lellinger, D.; Xu, D.; Ohneiser, A.; Skipa, T.; Alig, I. *Phys. Sta. Sol. B* **2008** 245, 2268-2271.
15. Li, S.N.; Li, B.; Li, Z.M.; Fu, Q.; Shen, K.Z. *Polymer* **2006** 47, 4497-4500.
16. Schuh, C.A. *Mater. Today* **2006**, 9, 32-40.
17. Oliver, W.C.; Pharr, G.M. *J. Mater. Res.* **1992**, 7, 1564-1583.
18. Cakmak, U.D.; Schöberl, T.; Major, Z. *Meccanica* **2012**, 47, 707-718.
19. Van Landingham, M.R.; Villarrubia, J.S.; Guthrie, W.F.; Meyers, F. *Macromol. Symposia* **2001**, 167, 15-43.
20. Pharr, G.M.; Strader, J.H.; Oliver, W.C. *J. Mater. Res.* **2009**, 24, 653-666.
21. Yao, C.K.; Liao, J.D.; Chung, C.W.; Sung, W.I.; Chang, N.J. *Appl. Surf. Sci.* **2012**, 262, 218-221.
22. Faruque, S.A.; Yi, J.W.; Moon, M.W.; Jang, Y.J.; Park, B.H.; Lee, S.H.; Lee, K.R. *Plasma Processes Polym.* **2009**, 6, 860-865.
23. Shokrieh, M.M.; Hosseinkhani, M.R.; Naimi-Jamal, M.R.; Tourani, H. *Polym. Test.* **2013**, 32, 45-51.
24. Chakraborty, H.; Sinha, A.; Mukherjee, N.; Chattopadhyay, P.P. *J. Nanotech.* **2012**.
25. Shen, L.; Phang, I.Y.; Liu, T.; Zeng, K. *Polymer* **2004**, 45, 8221-8229.
26. Wegrzyn, M.; Benedto, A.; Gimenez, E. *J. Appl. Pol. Sci.* **2013**, 131, 40271-40278.
27. Wegrzyn, M.; Juan, S.; Benedito, A.; Gimenez, E. *J. Appl. Pol. Sci.* **2013**, 130, 2152-2158.
28. Briscoe, B.J.; Fiori, L.; Pelillo, E. *J. Phys. D: Appl Phys.* **1998**, 31, 2395-2405.
29. Vega, J.F.; Martinez-Salazar, J.; Trujillo, M.; Arnal, M.L.; Müller, A.J.; Bredeau, S.; Dubois, P. *Macromolecules* **2009**, 42, 4719-4727.
30. Bokobza, L.; Zhang, J. *Express Polym. Let*. **2012**, 6, 601-608.
31. Gupta, M.; Wang, K.K. *Polym. Comp.* **1993**, 14, 367-382.
32. Abbasi, S.; Carreau, P.J.; Derdouri, A. *Polymer* **2010**, 51, 922-935.
33. Sahin, S.; Yayla, P. *Polym. Test.* **2005**, 24, 613-619.
34. Chasiotis, I.; Chen, Q.; Odegard, G.M.; Gates, T.S. *Exp. Mech.* **2005**, 45, 507-516.

35. Penumadu, D.; Dutta, A.; Pharr, G.M.; Files, B. *J. Mater. Res.* **2003**, 18, 1849-1853.

36. Briscoe, B.J.; Fiori, L.; Pelillo, E. *J. Phys. D* **1998**, 31, 2395-2405.

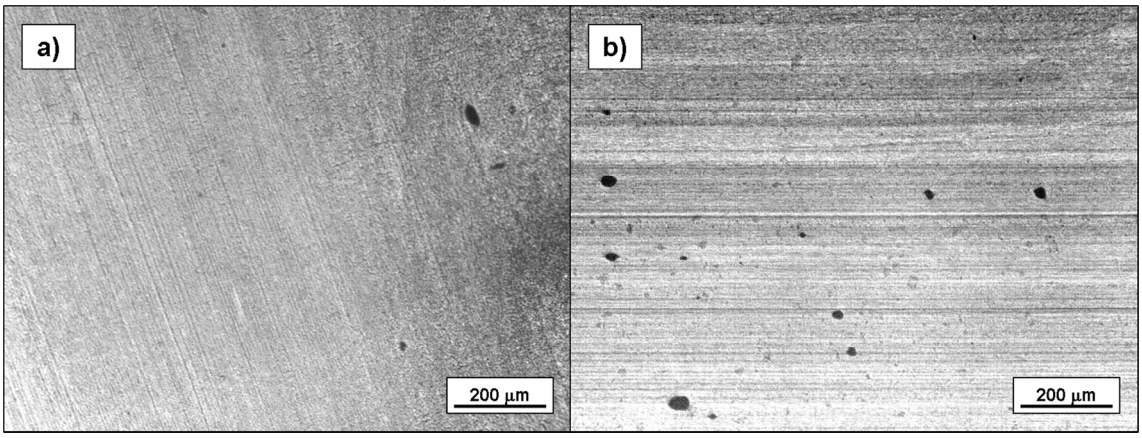

FIGURE 1: Transmitted light microscopy images from the central part of nanocomposite specimen (0.5 wt.% MWCNT) injection molded at: a) 25 mms^{-1} and b) 100 mms^{-1}.

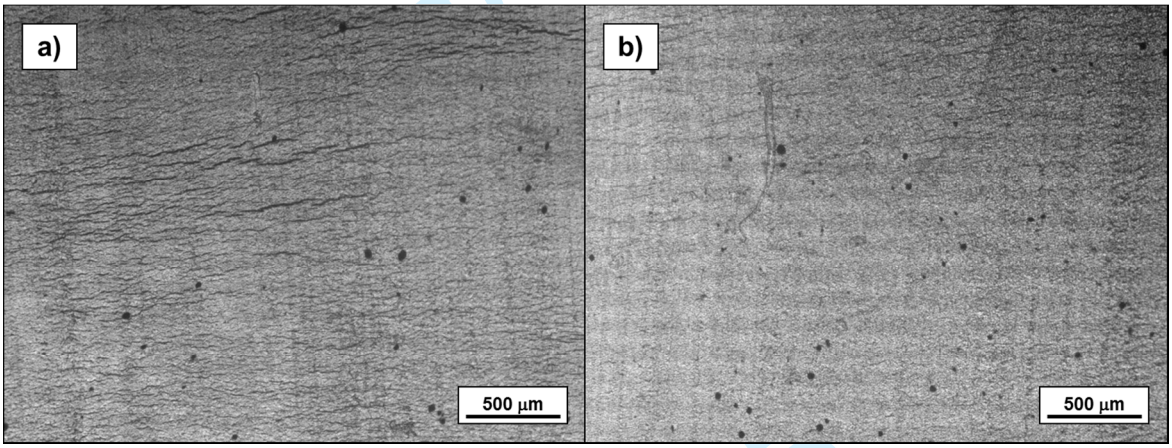

FIGURE 2: Transmitted light microscopy images from the central part of nanocomposite specimen (1.0 wt.% MWCNT) injection molded at: a) 25 mms^{-1} and b) 100 mms^{-1}.

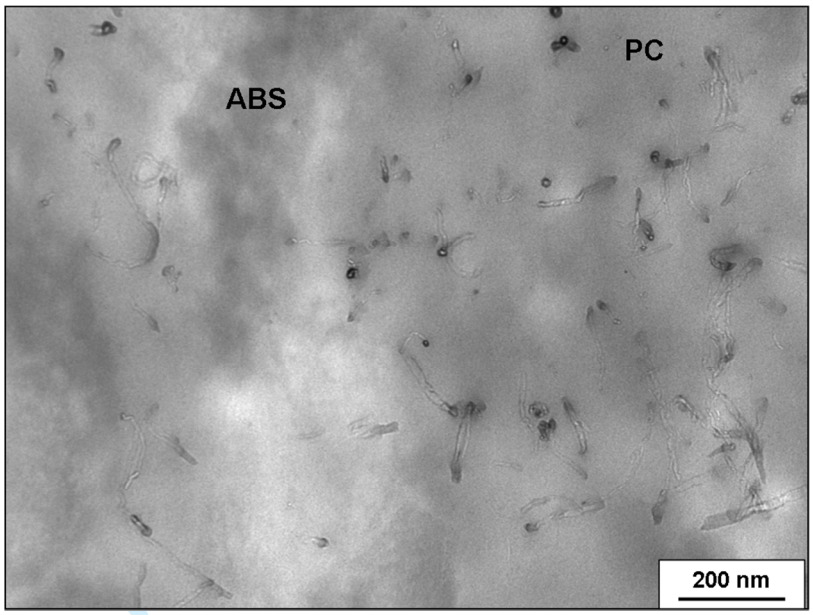

FIGURE 3: TEM micrograph of nanocomposite with 1.5 wt.% MWCNT injection molded at 100 mms^{-1}.

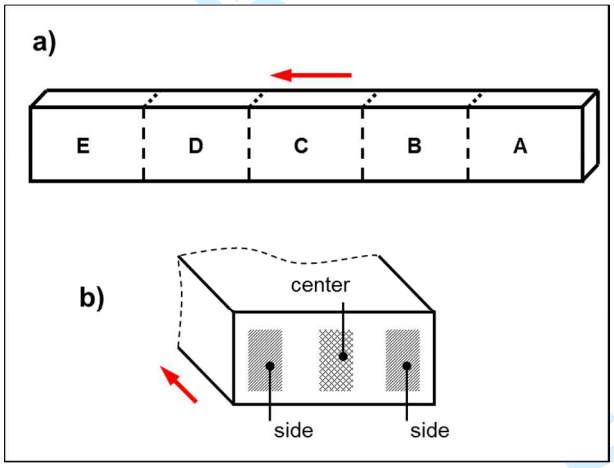

FIGURE 4: Scheme of sample preparation for Raman spectroscopy: a) cutting and b) measured points in the cross-section of each cut.

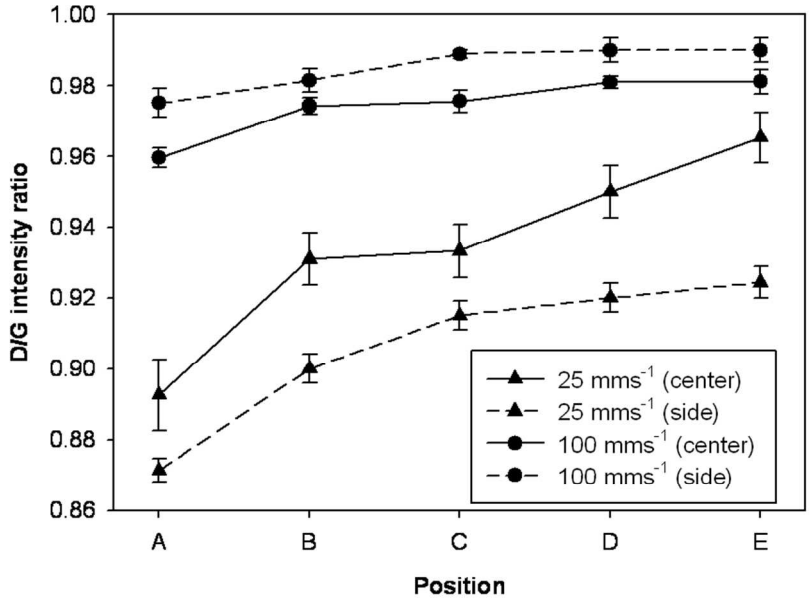

FIGURE 5: D/G intensities ratio difference recorded for nanocomposite 3.0 wt.% MWCNT injection molded at various conditions; legend relates to description of the cross-section.

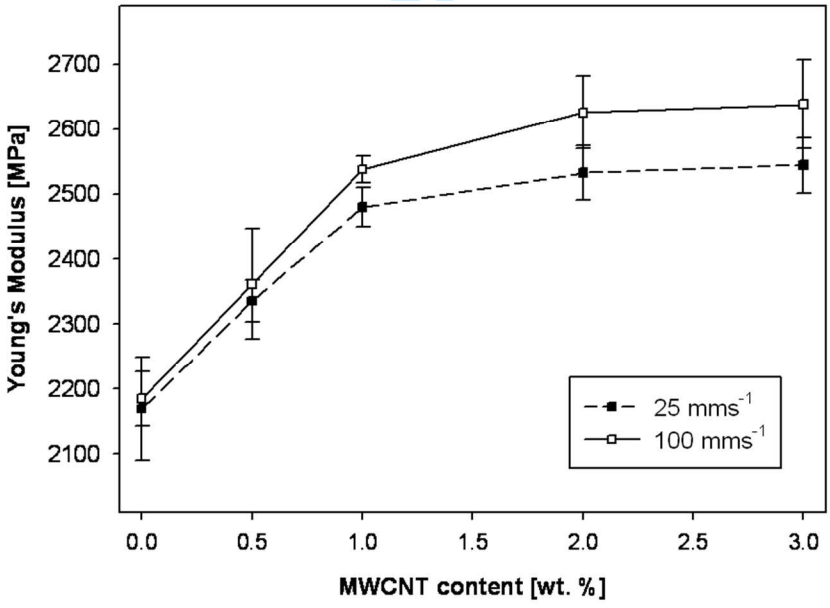

FIGURE 6: Young's modulus of injection molded PC/ABS-MWCNT nanocomposites obtained during tensile testing.

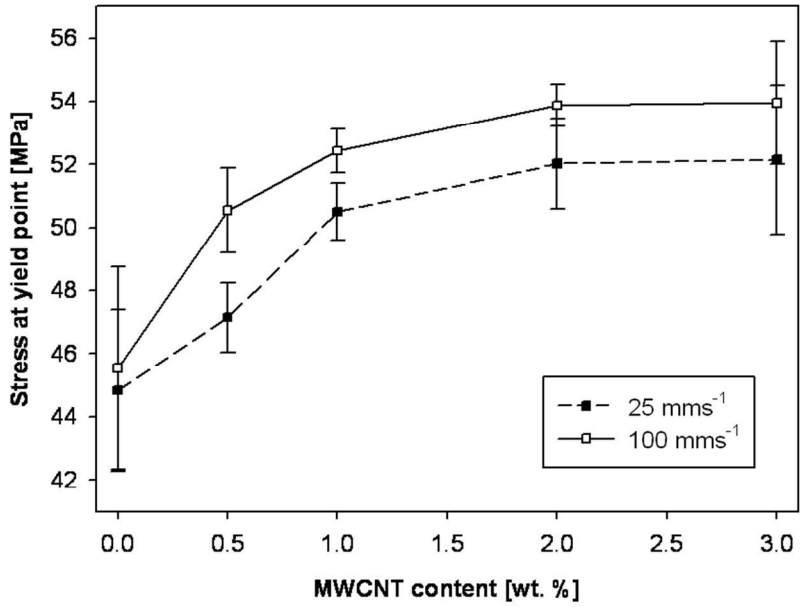

FIGURE 7: Yield stress of injection molded PC/ABS-MWCNT nanocomposites obtained during tensile testing.

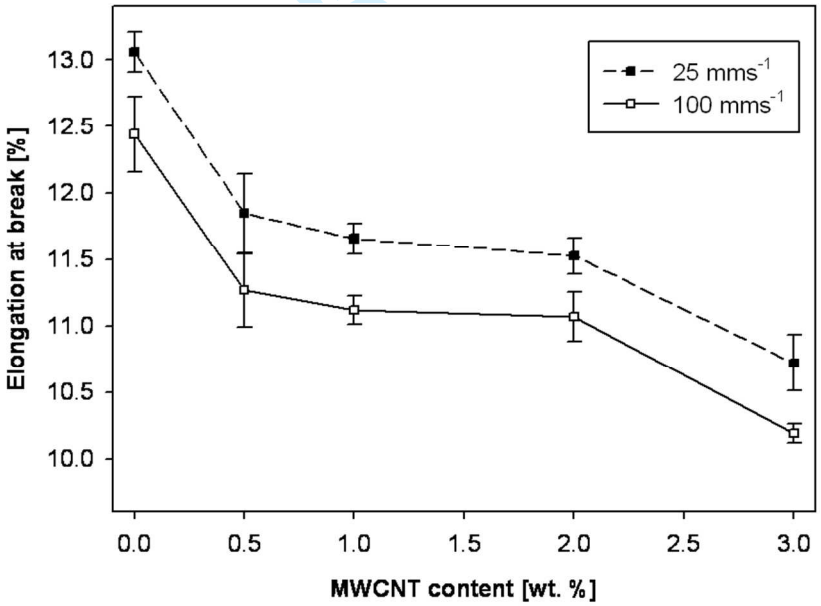

FIGURE 8: Elongation at break of injection molded PC/ABS-MWCNT nanocomposites obtained during tensile testing.

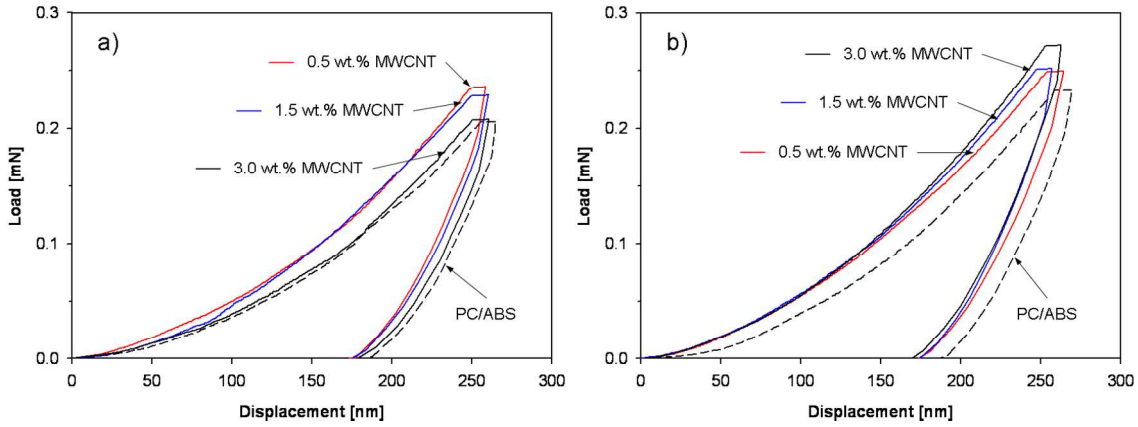

FIGURE 9: Typical loading-hold-unloading curves of neat PC/ABS and its nanocomposites injection molded at: a) 25 mms^{-1} and b) 100 mms^{-1}.

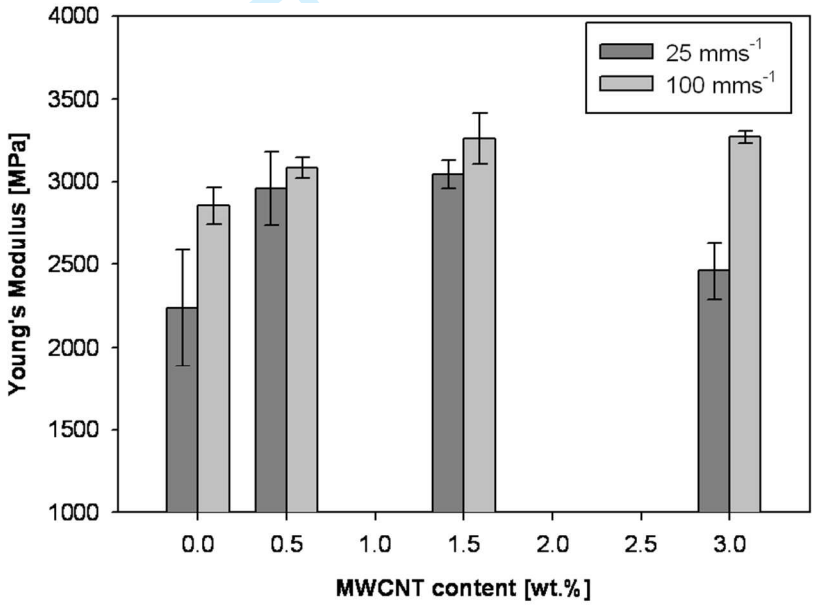

FIGURE 10: Young's modulus of injection molded PC/ABS-MWCNT nanocomposites obtained from nanoindentation measurements.

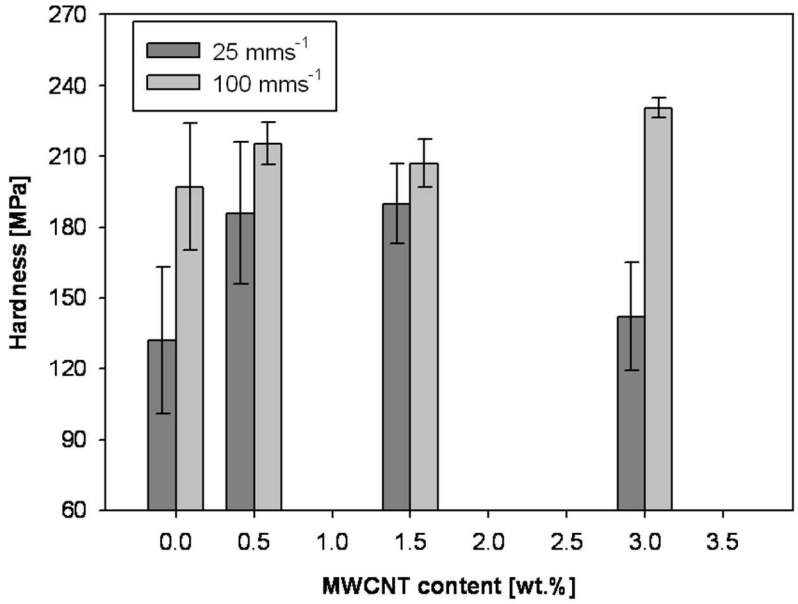

FIGURE 11: Hardness values obtained from nanoindentation test.

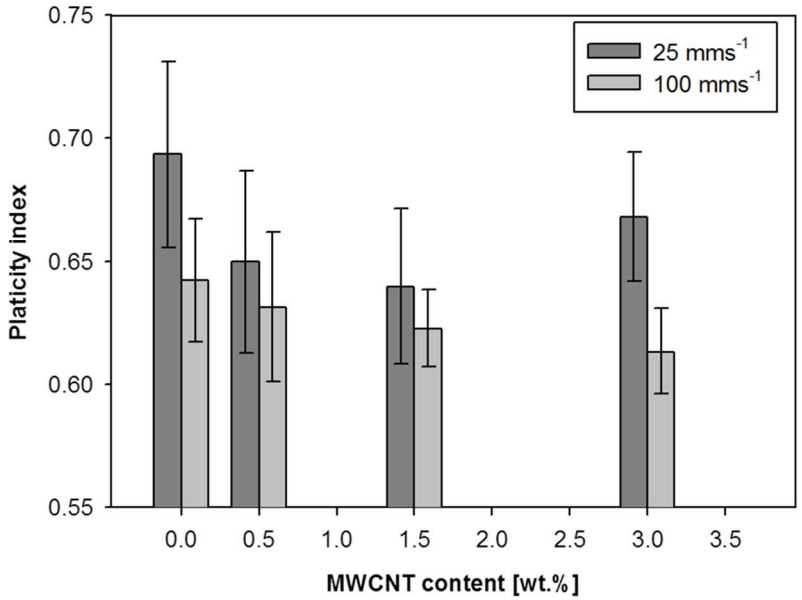

FIGURE 12: Plasticity index calculated from load-displacement curves.

Reviewer #1:

- The last sentence in the Abstract is changed now.
- This publication is focused on the mechanical performance of injection molding PC/ABS-MWCNT nanocomposites. Therefore, an extended description of the state of MWCNT distribution would be only a repetition from the previously published paper.

  Figure 3 shows clearly two phases being polycarbonate (PC) and ABS terpolymer. Carbon nanotubes present in Figure 3 appear as it commonly occurs in the related literature. Any additional changes done to this image could result with blurring the information that Figure 3 conveys.
- The first paragraph is now rewritten.
- The results regarding balance between the agglomerates coalescence efficiency and agglomerates destruction are published exclusively for mono-phase matrices. In immiscible matrices (like PC/ABS studied in this work) this balance may be distracted due to the additional variables introduced to the system (e.g. flow ability difference between PC and ABS). Besides that, the explanation given by the authors agree with the results from independent nanocomposite characterization methods.
- Declaration that the increase in viscosity of nanocomposite melt decreases “the number of freedom degrees of the individual carbon nanotubes" in now changed.
- Text in the "Nanoindentation results" is now changed and corrected.
- Explanation of discrepancy between results of the tensile test and nanoindentation is now corrected.
- Explanation of Figure 10 and Figure 11 is now straighten.
- English language has been corrected.

Reviewer #2:

- Reference for equation (1) is now added.
- Agglomerates size distribution and agglomeration behavior in PC/ABS-MWCNT nanocomposites are studied and described in details in cited publications (Wegrzyn, M. et al., *J. Appl. Pol. Sci.* **2013**, 131, 40271-40278 and Wegrzyn, M. et al., *J. Appl. Pol. Sci.* **2013**, 130, 2152-2158.)
- Concept of flow-induced agglomeration is described in publication: Liberatore, M.W. *J. Non-Newton. Fluids* **2003**, 113, 193-208.
- The authors in page 9 line 14-16 said: "higher orientation is caused by higher shear". However, the full sentence has different meaning, stating that the injection velocity

causes high shear between the frozen nanocomposite layer and the melted nanocomposite, and this could be the cause of nanotubes orientation in this region.